Multistatic Sensor Placement: A Tracking Approach

O. ERDINC

P. WILLETT
University of Connecticut

S. CORALUPPI
NATO Undersea Research Centre

Active sonar tracking using measurements from multistatic sensors has shown promise: there are benefits in terms of robustness, complementarity (covariance-ellipse intersection) and of course simply due to the increased probability of detection that naturally accrues from a well-designed data fusion system. It is not always clear what the placement of the sources and receivers that gives the best fused measurement covariance for any target—or at least for any target that is of interest—might be. In this paper, we investigate the problem as one of global optimization, in which the objective is to maximize the information provided to the tracker.

We assume that the number of sensors is given, so that the optimization is done in a continuous space. The strong variability of target strength as a function of aspect is integral to the cost function we optimize. Doppler information is not discarded when constant frequency (Doppler-sensitive) waveforms are available. The optimal placements that result are consistent with our intuition, suggesting that our placement strategy may provide a useful tool in more complex scenarios where intuition is challenged.

Manuscript received July 3, 2007; revised November 11, 2007; released for publication December 4, 2007.

Refereeing of this contribution was handled by Robert Lynch.

This research was supported by the Office of Naval Research under contracts N0014-04-1-0133 and N0014-07-1-0055. This paper is a significantly expanded version of [7], itself a development on [6].

Authors' adresses: O. Erdinc and P. Willett, Electrical and Computer Engineering Department, University of Connecticut, Storrs, CT, Email: {ozgur,willett}@engr.uconn.edu.; S. Coraluppi, Reconnaissance, Surveillance, and Networks Department, NATO Undersea Research Centre, Viale S. Bartolomeo 400, 19138 La Spezia, Italy, Email: coraluppi@nurc.nato.int.

1. INTRODUCTION

A. Background

Multistatic sonar networks have the potential to improve anti-submarine warfare (ASW) detection and tracking performance against small, quiet targets in harsh reverberation-limited littoral operating areas. This improved performance comes from increased area coverage, expanded geometric diversity (greater coverage footprint), increased target hold, robustness to sensor loss and jamming, improved localization through cross-fixing (complementarity of uncertainty); and of course through simple gains in probability of detection via data fusion [5].

Moreover, multistatic systems are flexible. It is possible to use different waveforms at different sources, and the ping times can be chosen with greater freedom. In most scenarios, how to choose these parameters to exploit the capabilities of the multistatic sonar system is not immediately obvious—flexibility brings complexity. In practice it is common that parameters such as sensors' locations, waveforms and ping times are chosen heuristically and perhaps not optimally.

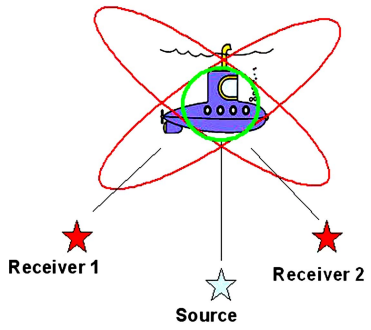

Fig. 1. Cartoon illustrating one of the benefits of using multistatic sonar: complementarity of the localization uncertainties.

In this paper, we investigate the advantages that an optimized sensor placement might offer, and we propose a methodology to determine the optimal placement strategy. Tracking in a complex and time-varying ocean environment is challenging. Multi-path effects, salinity/temperature gradients and geographical constraints may result in highly cluttered and/or low SNR sonar signals. Hence, finding the "best" placement strategy is going to be a considerable help to the tracker. In this work, it is assumed that quickly-deployable short range sensors are used and based on the predicted tracking performance, a sensor re-deployment scheme is proposed.

This study began with [6], which introduced many of the features from this paper (a similar criterion, aspect dependence, blanking zone). In [6] a certain intuitive regularity in optimized sensor layout was noted, and the incremental benefit of complementarity between sensors' perspectives (intersecting covariance ellipses)

was seen to diminish after the second source/receiver pair. The results were considerably more stable in [7], presumably due to the use of the *minimax* optimization that we shall discuss shortly. The current paper is more comprehensive, and additionally considers the case of Doppler-sensitive waveforms. We find the work of Hernandez and Horridge [10], [11], who use the posterior Cramer-Rao lower bound (PCRLB), highly relevant. The PCRLB is dynamic and allows for both missed detections and false alarms by incorporating the information reduction factor (IRF) [12]. A question answered in [10] is: Given a present target being tracked and its associated uncertainty, where ought a new sensor be "dropped" to minimize the future uncertainty? In this paper we have a different concern: How should a field of sensors be configured to protect against an intelligent threat? The PCRLB is perhaps a better indication of tracking performance than the metric we shall introduce; but as noted in [10] it is more complex, conservative, and requires a description of the target dynamics and initial uncertainty.

In the next section, we explain our modeling assumptions. Then, we outline the proposed optimization technique, while Sections 4 to 7 report representative results. In the final section, we summarize our contribution.

B. Deployable Experimental Multistatic Sonar (DEMUS) System

We relate our analysis to DEMUS [14], an experimental system designed and used for investigation of the potential of multistatic sonar systems. The DEMUS system is composed of three deployable receiver arrays and one deployable acoustic source. Each system is battery powered, moored to the sea bottom, and communicates with the ship via radio and satellite links sited on a surface buoy. The receiver array records 64 channels of acoustic data (7 arms of 9 staves, plus one in the center). Each vertical stave sums the output of 3 hydrophones. The array's aperture may be scaled by extending the system's arms. The source array is made up of a vertically suspended set of 8 free flooded acoustic rings, capable of transmitting at high power.

Bistatic sonar can have many configurations, and the characteristics of DEMUS, our notional platform, include its relatively large beamwidth (approximately six degrees)—although with sufficient SNR the angular resolution can be made much better via interpolation—and the isotropic nature of its angular resolution. That is, although many sonar arrays have different performance depending on their orientation (e.g., broadside versus endfire in a linear array), DEMUS does not: this removes a parameter from our optimization process and allows us to concentrate on placement alone. In other words, the optimization is done concerning the locations of the sensors, their orientations do not matter.

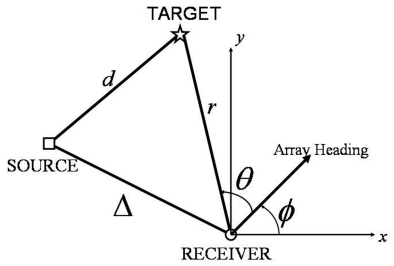

Fig. 2. Bistatic source/receiver/target geometry for a single source/receiver pair.

2. MODELING

A. Measurement Model and Localization Accuracies

In active sonar, the measurements are the return of the transmitted acoustic signal from the target of interest and the time of arrival. Hydrophones (receivers) determine the angle of arrival that gives the localization of the target together with the traveling time of the signal. Further, the transmitted frequencies could be translated from those of the received signal due to the relative motion of the target to the source and/or receiver. This Doppler shift provides information on the relative speed of the targets. In this paper we assume two different cases: first, with Doppler information not available, specifically where a wide-band linear frequency modulated (LFM) sonar signal is used; and second, a constant frequency sonar signal (CW) is used and Doppler information incorporated in the localization analysis.

The measurement model for a multistatic system, with stationary source and receiver, is

$$\begin{bmatrix} r \\ \theta \\ \dot{r} \end{bmatrix} = \begin{bmatrix} r_{tr} \\ \tan^{-1}\left(\dfrac{y-y_r}{x-x_r}\right) \\ \dfrac{\dot{x}(x-x_s)+\dot{y}(y-y_s)}{2r_{ts}} + \dfrac{\dot{x}(x-x_r)+\dot{y}(y-y_r)}{2r_{tr}} \end{bmatrix} + w, \quad w \sim \mathcal{N}(0,\Sigma) \tag{1}$$

where the target state consists of its position and velocity, $X_t = [x \;\; y \;\; \dot{x} \;\; \dot{y}]'$ and r_{tr} is the range between the target and the receiver. For LFM signals, the range rate measurement $\dot{r}$ is insignificant and hence ignored.

The localization accuracy, i.e. the covariance matrix of the target state estimation after a single observation set $[r \;\; \theta \;\; \dot{r}]'$ is received, is a function of source, receiver, and target states and the selected sonar waveform,

$$R(X_s, X_r, X_t, \omega) = \begin{bmatrix} \sigma_x^2 & \sigma_{xy} & 0 & 0 \\ \sigma_{xy} & \sigma_y^2 & 0 & 0 \\ 0 & 0 & \sigma_{\dot{x}}^2 & \sigma_{\dot{x}\dot{y}} \\ 0 & 0 & \sigma_{\dot{x}\dot{y}} & \sigma_{\dot{y}}^2 \end{bmatrix} \tag{2}$$

where

- X_s: source's state (location) in Cartesian plane, $s = 1, 2, \ldots, N_s$, N_s is the number of sources.

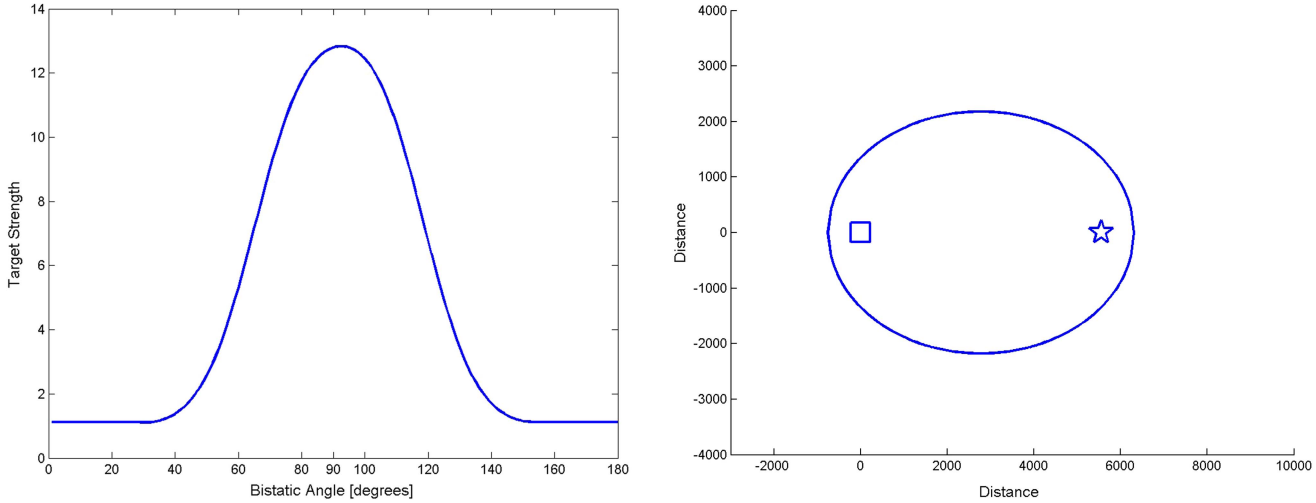

Fig. 3. Left: Nominal target strength [in dB] versus bistatic angle. Specular reflections from the broadside of the target are expected to be considerably stronger than those from oblique or endfire angles. Right: The blanking zone ellipse, with source indicated by the box and receiver by the star. Target detection is not possible within the blanking zone.

- X_r: receiver's state (location) in Cartesian plane, $r = 1,2,\ldots,N_r$, N_r is the number of receivers.
- X_t: target's state (location and velocity) in Cartesian plane.
- ω: selected waveform, $\omega \in \{\text{LFM, CW}\}$.

In recent work [3], [4], localization errors for bistatic and quasi-monostatic contact localization accuracy were derived as a function of the source-target-receiver geometry and assumed error statistics for source and receiver locations, sound speed, time, bearing, and array heading measurements. This study illustrated that the impact of measurement errors on localization accuracy depends highly on the source-target-receiver geometry. Due to space limitations we omit the lengthy equations showing the relations between the errors mentioned above and the components of covariance matrices, and refer the interested reader to the related publications [3] and [4]. Coraluppi has described the measurement errors and, more important, the measurement error covariances, as a function of the fundamental system errors in angle, observation time, array orientation, speed of sound and source receiver locations. Sensitivity analysis of these errors can be found in a consequent publication [9].

B. Target Detection Modeling

In addition to the localization analysis a second element that we require in the optimization metric to be discussed in Section 3-A is a model for target detection capability. Significant work exists on elaborate target strength and signal-to-noise (SNR) modeling; we have chosen to work with simple models that capture the key geometric dependencies relevant to CW and LFM transmitted waveforms.

1) *Aspect Dependence*: In many studies, targets are assumed to be a *point*: the sonar cross-section is independent of the angle of illumination; or, in the case of bistatic systems, independent of the relative angle between source and receiver. Many practical targets do not have this behavior at all. A "specular" return from a target whose broadside is normal to the bistatic angle is apt to be much larger than from a target that presents some other visage. Much is known about some targets. However, to keep our work generic, yet still to capture a flavor of the aspect-dependence that we seek, we have applied a simple target strength (TS) model to represent the aspect angle dependence of the signal return. If the target heading happens to be parallel to the line between the source and the receiver, the target strength is highest. This effect degrades as the angle varies away from the "best" angle; i.e., 90 degrees. Fig. 3 shows the target strength versus bistatic angle. If the expected target heading is known (for example, the surveillance volume is a narrow region that any target must traverse), the sensor placement ought to exploit this information.

2) *Direct Blast*: An important concern in bistatic systems is the direct blast: the signal that arrives at the receiver via the direct path. Propagation speed dictates that no target's return can arrive at the receiver prior to the direct blast; but, more important, since the direct blast is considerably louder than any target reflection, as a practical matter no reception is possible until the direct blast passes over. The direct blast can be very useful in calibration and registration, and consequently is perhaps a great strength of the multistatic architecture. However, there is an unavoidable "blanking zone" (the inside of an ellipse having source and receiver as foci and whose target-locus-receiver distance is the transmitted pulse length times the speed of propagation) as illustrated in Fig. 3, in which the system is blind.

3) *Signal-to-Noise Ratio (SNR) Modeling*: It is assumed that the multistatic system will be capable of transmitting and processing both LFM and CW. This capability is desired in a multistatic system since LFM and CW waveforms are "complementary." When the

target strength is maximum, target heading is parallel to the line between the source and the receiver, the target is in Doppler blind zone, i.e. range rate remains the same no matter what the target speed is. In this situation LFM waveform (or any Doppler-insensitive waveform) would be the right choice to use. On the contrary, when the target heading is perpendicular to bistatic orientation, then the target strength is minimum, whereas the range-rate is highest. Hence, a Doppler-sensitive waveform such as CW would provide high SNR.

In [8], SNR is calculated as a function of source/receiver/target locations and the selected waveform by a model that employs a simplified reverberation-limited sonar equation and a Q-function, which quantifies Doppler performance of sonar waveforms in rejecting reverberation. The model allows for both CW and LFM waveforms, and is sensitive to a number of waveform properties including center frequency, bandwidth, etc. In our work, we use this model and the reverberation-limited active sonar equation becomes (see [8] for details),

$$\mathrm{SNR} = \mathrm{TS} - \mathrm{BSS} - \mathrm{AREA} - Q(\Delta_f) \tag{3}$$

where TS is the target strength (as in Fig. 3-left), BSS is the bottom scattering strength, a parameter that depends on ocean seafloor type and composition (for our purposes, this is constant over the surveillance region), AREA is the area of the ensonified patch (i.e., resolution cell) that is a function of beam-width and the range from receiver to the patch, and the last term, $Q(\Delta_f)$, is the (negative-valued) Q-function, which reduces the amount of reverberation energy as a function of the target's Doppler shift. $Q(\Delta_f)$ is the term that quantifies Doppler-sensitive constant-frequency (CW) waveform's advantage over the FM waveform.

4) *Target Detection Probability and Detection-Localization Coupling*: The target detection probability for source i, receiver j, and waveform w, assuming Swerling I model (i.e., Rayleigh distributed target amplitude), is given by [13]

$$P_d^{\omega}(i,j) = e^{-DT/(1+\mathrm{SNR})} \tag{4}$$

where DT stands for the detection threshold. We set DT at 10 dB. The measurement error assumptions that drive the state estimation covariance (see equation 2) calculations include bearing, timing and frequency shift errors; these are related to the observed SNR as follows:

$$\sigma_\theta = \frac{\lambda}{\sqrt{\mathrm{SNR}}} \tag{5}$$

$$\sigma_\tau = \frac{\gamma}{\sqrt{\mathrm{SNR}}} \tag{6}$$

$$\sigma_f = \frac{\zeta}{\sqrt{\mathrm{SNR}}} \tag{7}$$

where λ, γ, ζ are some constants. This implies that amplitude-weighted interpolation between beams and between matched-filter bins is performed [2]. This coupling is used in our optimization work; that is, for each source-target-receiver geometry, we determine the measurement error standard deviations to be employed.

3. SENSOR PLACEMENT OPTIMIZATION

In this section, we describe the details of the proposed optimization algorithm. We propose an objective function that utilize the state estimation covariance matrix, R, and the probability of detection, P_d. The bearing, timing and the frequency errors that are used in the calculation of R, depend on the SNR value. Hence, R is a function of target orientation, relative Doppler, and source, receiver, target locations; so is P_d.

A. Objective Function

In finding an optimal sensor placement, our main objective is to improve target tracking performance. Hence, we use the "information" flow to the tracker as the basis of the optimization surface. The Fisher information matrix can be seen as a quantification of information in the measurement about the target's state. In Section 2-A, we have shown that the target localization uncertainty R can be derived as a function of source/receiver/target locations and the selected waveform (CW or LFM). The Fisher information matrix is defined as the inverse of the covariance of the estimate:

$$I(X_s, X_r, X_t, \omega) = R(X_s, X_r, X_t, \omega)^{-1}. \tag{8}$$

For optimization purposes, we need a scalar quantity for each source, receiver and target configuration for a given waveform ω (CW or LFM). We use the "information gain"

$$I_{\mathrm{fused}}(X_t) = \sum_{\forall \omega} \sum_{\forall (s,r) \in Y} P_d^{\omega}(s,r) I(X_s, X_r, X_t, \omega). \tag{9}$$

$I_{\mathrm{fused}}(X_t)$ is a function of target location given a particular geometry Y—the locations of sources and receivers, see (14). In other words, the second sum in the equation (9), implies that all source/receiver pairs' locations in the given geometry are considered. Note that equation (9) is based on the simplifying approximation that sensor measurement errors are uncorrelated from one contact to another, and indeed can be related to the PCRLB [10] for the case of a target without process noise and in the absence of false alarms. This is true for contact timing and bearing errors, but is not the case for source and receiver positioning errors, array heading errors, and speed of sound errors. Thus, the expression, while simple and useful for our purposes, has some degree of optimism: the true information gain is upper bounded by this expression.

Direct blast blanking means that for certain source-target-receiver geometries the detection probability that

follows from our signal-excess modeling must be replaced by zero. Rather than doing so, and for numerical stability in the optimization process, we choose instead to discount the information gain with a barrier-type function. That is, as the target moves into the direct blast region, it is still detected but with a rapidly increasing localization uncertainty:

$$I(X_s, X_r, X_t, \omega) = e^{-\kappa d} \cdot I(X_s, X_r, X_t, \omega) \tag{10}$$

where d is the shortest distance between the target and the border of the blanking zone ellipse.

We choose the determinant to be the scalar measure of the quality of information available to the tracker at each waypoint. Moreover, we consider a set of linear target trajectories T, each consisting of several waypoints, as illustrated in Fig. 4. The number of waypoints along each trajectory differs based on the speed of the target and the sampling interval; the latter is chosen so as to have several waypoints for the fastest-moving trajectories of interest. We use the (optimistic) simplifying approximation that information gained along a trajectory is the summation of the information across waypoints. Thus, as the scalar measure for each trajectory $T_i \in T$, we use the summation of determinants of the fused information matrix over all waypoints $w_{ij} \in T_i$:

$$M(T_i) = \sum_j \det(I_{\text{fused}}(w_{ij})). \tag{11}$$

The objective function may be defined in either an *average* or *worst-case* sense. The former approach seems more applicable to problems where surveillance assets are covert, and is defined as:

$$J = \sum_i M(T_i) \tag{12}$$

where i is the trajectory index. Alternatively, the objective function J can be defined as the *worst-case* (i.e. smallest) information gain achieved across all trajectories:

$$J = \min_i M(T_i). \tag{13}$$

Maximization of the latter objective function is in fact the well-known *minimax* criterion: minimization of the maximum possible loss. In an overt network, a threat submarine would try to choose a path so that it would not be detected. Hence, operationally, the minimax criterion makes more sense since it makes sure that there are no "holes" in the surveillance region. We choose it as our objective in the optimization.

Note that this objective incorporates (and maximizes) both localization accuracy and the detection opportunities over the whole trajectory of the target. In other words, it aims to improve the tracking accuracy at all instances of target penetration. Hence, it can be seen that it relates to other operationally meaningful objectives, such as maintaining (not losing) a track, or increasing the target detectability.

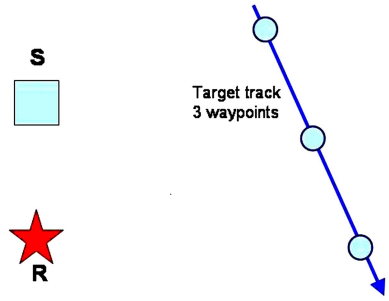

Fig. 4. In optimization, target trajectories are used instead of target grids. A target heading south-east is shown, with 3 waypoints along its trajectory.

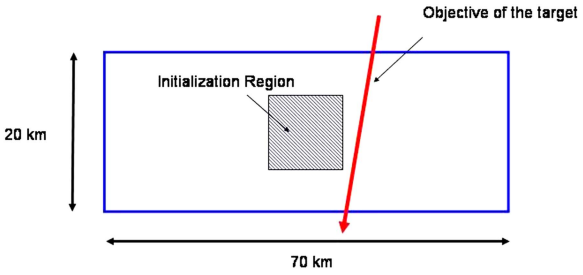

Fig. 5. Barrier Scenario: the best placement should prevent any target from passing this 20 km-by-70 km barrier without being tracked. The sensors are initially randomly placed inside the shaded region.

B. Our Scenario

Here we consider the barrier-scenario; the target submarine aims to pass a barrier 20 km long and 70 km wide (see Fig. 5). The multistatic sonar system has to be placed optimally so that no target can pass this region without being tracked. We consider some possible target trajectories, where the target heading and the speed differ (see Fig. 7; solid lines show 15 different trajectories). The objective is to maximize the provided information in the worst target trajectory. Operationally, the surveillance area should have no "holes." The tracker's performance is expected to meet some requirements even in the worst cases.

C. Likelihood Surfaces

With N available sensors, the parameter space for the optimization algorithm is $2N$, reflecting the need to locate each sensor in both latitude and longitude. We have no particular prescient knowledge on how this $2N$ dimensional surface would look, and hence it is not easy to decide on the most appropriate optimization algorithm. However, we can take 2-dimensional snapshots from this surface. One example is given in Fig. 6. The dark colored area around $(8000, -10000)$ is the best placement for the 3rd receiver at the moment that the snapshot is taken. In this figure, this snapshot reveals a smooth surface, although one that is not necessarily concave. We choose the steepest ascent algorithm, mainly

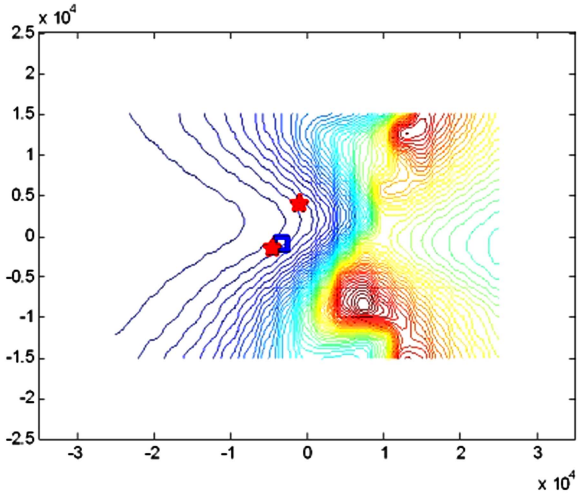

Fig. 6. 2-dimensional snapshot of 8-D surface: 1 source and 2 receiver positions are held, the 3rd receiver is free. The best positions are dark red areas at right.

since it is easy to implement, and it is intuitively easy to monitor its behavior.

D. Steepest Ascent Algorithm

The steepest ascent algorithm is a gradient-based unconstrained optimization technique. Y is a stacked vector of dimension $2N$,

$$Y = [X_{s_1} \; X_{s_2} \cdots X_{s_{N_s}} \; X_{r_1} \; X_{r_2} \cdots X_{r_{N_r}}]' \tag{14}$$

where total number of sensors is $N = N_s + N_r$. In each iteration k, Y^k moves in the direction of the gradient of the objective function, until convergence to a (local) maximum occurs. We have

$$Y^{k+1} = Y^k + \alpha^k \nabla f(Y^k) \tag{15}$$

where α_k is the step size used at iteration k. As previously described, we use objective function

$$f(Y^k) = J = \min_i \sum_j \det(I_{\text{fused}}(w_{ij})) \tag{16}$$

where $i = 1, 2, \ldots,$ *number of waypoints*. Due to the complicated nature of the objective function, $f(Y^k)$, it is hard to obtain the gradient analytically. Hence a numerical gradient evaluation scheme is used. We approximate the gradient at the direction i by the central difference formula [1],

$$\frac{\partial f(Y^k)}{\partial Y^i} \approx \frac{1}{h}(f(Y^k + he_i) - f(Y^k - he_i)) \tag{17}$$

where h is fixed for each gradient direction and the e_i is the unit vector in the direction of Cartesian basis vector i. The value of h should be chosen as small as possible, otherwise, the coarsely-discretized objective function may result in erroneous gradient estimates. On the other hand, smaller h may cause numerical problems near the local maximum [1].

Step-size selection is a critical step for fast convergence.[1] The step-size needs to be large enough to reach the local minimum soon, and small enough to prevent oscillation (or large errors) when near the critical point. We apply a successive step-size reduction strategy, the so-called "Armijo rule" [1]. The Armijo rule picks its step-sizes to satisfy the inequality

$$f(Y^k) - f(Y^k + \beta^m s \nabla f(Y^k)) \geq -\sigma \beta^m s \|\nabla f(Y^k)\|^2 \tag{18}$$

where $0 < \beta < 1$ (chosen as $\beta = 0.7$), $0 < \sigma < 1$ (chosen as $\sigma = 0.1$), $s < 1$ and $m = 0, 1, 2$. The step-size is $\alpha_k = \beta^m s$. The Armijo rule first tests step-size s (i.e., $m = 0$) and then keeps increasing m until the inequality is satisfied. The parameter s (chosen as $s = 0.1$) and σ assure that there is a substantial increase in the objective function for the stepsize α_k. Convergence is declared when m reaches 20, this implying that the algorithm tests a point very close to the current one and there is still no improvement in terms of the objective. We choose s so that the first test point in the gradient direction would be 5 km away from the current location Y^k. Overall, the optimization algorithm works as follows:

1) Randomly initialize the sensors positions.[2]
2) Evaluate $f(Y^k)$ for current position vector Y^k.
3) Evaluate gradient by central difference formula ($2N * 2 = 4N$ $f(Y^k)$ evaluations.)
4) Test step sizes, α^k, according to Armijo rule. (At most m function evaluations.)
5) Update sensor positions using equation (15).
6) Go to step 2.

4. PLACEMENT STRATEGIES WITH LFM WAVEFORMS

We refer to a source-receiver pair as a detection node. In this section, we will consider 2-node and 3-node systems. Besides the main question of how to place these assets, we also aim to address which one of, for instance, the 2-node systems perform better? Is it better to deploy two sources with one receiver, or is the system with two-receivers and a source good enough? The barrier is the region $(-35$ km, -10 km) to (35 km, 10 km); there are 15 hypothetical target trajectories considered along this barrier. For instance, trajectory 1 represents a target with heading 200 degrees (from North) and 10 kts speed. Along this trajectory, there are 5 waypoints.

[1] We omit the discussions regarding the convergence rate of the steepest ascent algorithm. For a detailed analysis on the subject, see [1].

[2] Steepest ascent is not a stochastic method. Random initialization is hence important. It ensures that there is no bias in the convergence results.

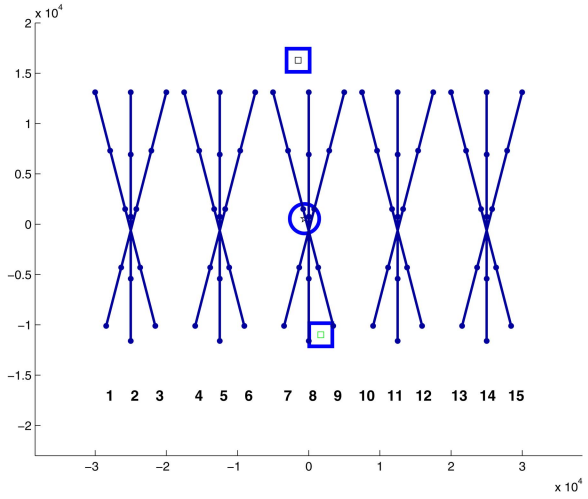

Fig. 7. 2 Sources (the squares), 1 Receiver (the circle) case: The lines are trajectories and the dots represent waypoints of each trajectory. Targets head south. The optimal placement forms a line in the North-South direction. See Table I for scores of trajectories.

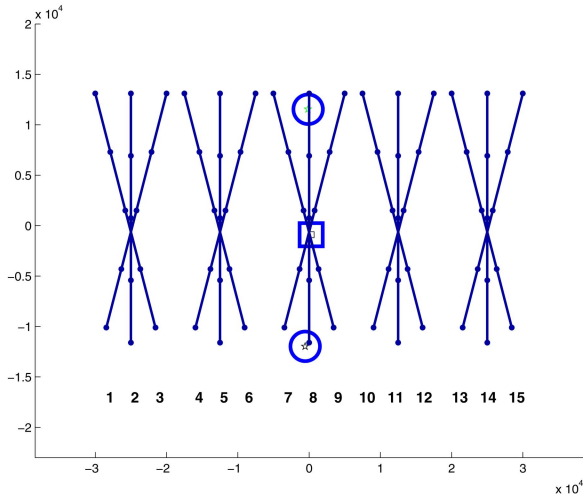

Fig. 8. 1 Source, 2 Receivers case: The optimal placement is very similar to the one in Fig. 7. See Table I for scores of trajectories.

A. Two-Node Cases

We consider two 2-node systems: one source and two receivers, and two sources and one receiver. The optimal placement turns out to be that the sources (blue squares in the Figs. 7 and 8) and receivers (circled star in the Figs. 7 and 8) form a line in the North-South direction. This is intuitive since it allows sensors to see the target from broadside. As explained in Section 2-B1, the target strength is at its maximum if the bistatic angle is close to 90 degrees (i.e., broadside), meaning that the SNR is high. Moreover, the receivers are located so that for any given target location, the orientation of the uncertainty ellipses becomes complementary (see Fig. 1). These lead both to high P_d and to good localization accuracy, hence resulting in good fused information. The objective of maximizing the worst-case information gain leads to a "balanced" deployment solution. During the optimization process, the worst trajectory jumps between the west-most group to the east-most group. Hence, the convergence geometry ends up being in the middle of the barrier.

TABLE I
Scores of Trajectories of Figs. 7 and 8
(worst cases are shown bold)

Trajectories	2S-1R	1S-2R
1	68.17	68.56
2	70.24	72.46
3	71.60	73.83
4	42.50	42.96
5	43.95	46.27
6	37.86	42.83
7	56.43	71.19
8	55.75	58.01
9	40.73	48.30
10	39.15	43.34
11	42.76	43.88
12	44.23	41.65
13	**71.62**	**74.42**
14	71.32	73.68
15	71.13	70.53

Placement scores[3] are obtained by using

$$\text{score} = \sqrt{\frac{\sqrt{1/J}}{\pi}}. \tag{19}$$

Note that if a trajectory consists of a single waypoint (target grid), and assuming the R is round, i.e., it is a circular uncertainty around the target position, the score has a physical meaning: it is the radius of the $1-\sigma$ covariance circle.

Scores corresponding to the trajectories shown in Figs. 7 and 8 are given in Table I. Balanced deployments are evident from the scores (compare the scores of 1, 2, 3 with 13, 14, 15). Another intuitive outcome is apparent from the scores of trajectories 7, 8 and 9: For the single source case, they are higher (worse). When the target penetrates into the blanking zone of the first source/receiver pair, the range between the target and the receiver of the second S/R pair is significantly higher than in the case of 2 sources and 1 receiver. A higher range results in higher localization error, mainly due to the bearing error. So for an LFM waveform, it is better to deploy two sources and a receiver, given the we have only three assets.

B. Multiple-Node Case

We now consider the case that there are 3 receivers with a single source. Fig. 9 shows the outcome of the optimization algorithm. The optimal placement suggests to use a regular geometry that one might find "heuristic." However this solution is not unique. The differ-

[3]Note that the scalar metric used in optimization is the determinant. Score is introduced for easy comparison.

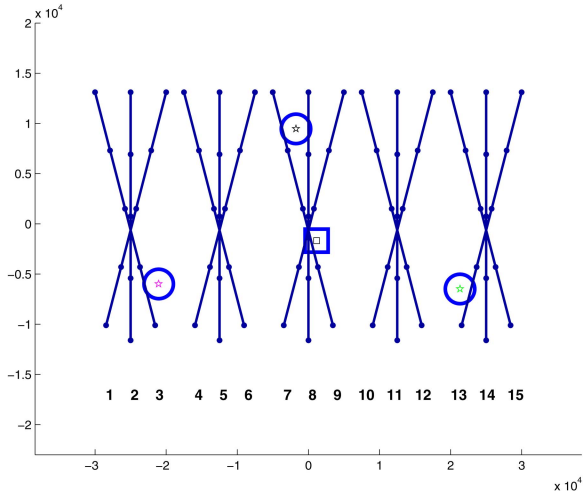

Fig. 9. 3 Receivers, one source case, the optimal placement: Two of the receivers (circles) are spread out to "monitor" the borders, and the source (square) is in the middle with the third receiver is in its north. They form a regular triangular geometry.

ent (random) initial placements result in different "optimal" placements, but they are equivalently good (see the scores from Table II).

It is intuitive that given a solution one can create its symmetric version and achieve the exact same scores in reversed order. Two such solutions are shown in Fig. 10. The initial placements were chosen randomly, but interestingly, the converged geometries are almost mirrored copies of each other. The scores indicate the reversed-ordering effect, and these solutions are as good as the regular-looking one from Fig. 9. Another nice feature is that the range of the scores is not wide, meaning that any path in the barrier would be monitored similarly. This is due to use of the minimax criterion.[4]

[4]Our observation is that another candidate criterion, maximizing the average measure, $\sum_i M(T_i)$, does not necessarily have this behavior. It can achieve an improvement in the average score by only improving some of the trajectories. Such a result would be operationally undesirable.

It is important to note that the steepest ascent algorithm is such that there is no guarantee that convergence is to the global optimum except when the objective function is concave; and from Fig. 6, we cannot assume a concave surface. Hence, our "optimal" solutions are not outcomes of each and every execution of the proposed algorithm. In fact, they are chosen so that they give the best score(s) among many runs of the optimization program. We follow this procedure:

- Execute the optimization process several times (on the order of 10).
- List all convergence scores.
- Determine distinct outcomes with scores close to the best overall score. (The optimal placements result in similar scores, and these scores are much lower than those in the rest of the list. Clustering is done by observation.)
- Ignore suboptimal placements.

It is important to note that all of the optimal placements yield "equivalent" solutions. In other words, they are very similar if one considers rotations and mirror reflections. The solutions given in Fig. 10 are an example for two such placements.

5. PLACEMENT STRATEGIES WITH CW WAVEFORMS

As opposed to an LFM waveform, a pulse at a constant frequency has coarser time resolution, and consequently, position-only estimation using only CW waveform yields a comparably larger uncertainty. On the other hand, a CW waveform provides Doppler information that is a function of the relative velocity of the target. Hence, while a fast target (e.g. 10 kts) yields few waypoints across the barrier, it is more likely to be detected when a CW waveform is used.

Since the information matrix has velocity uncertainty, the score loses its physical meaning when a CW

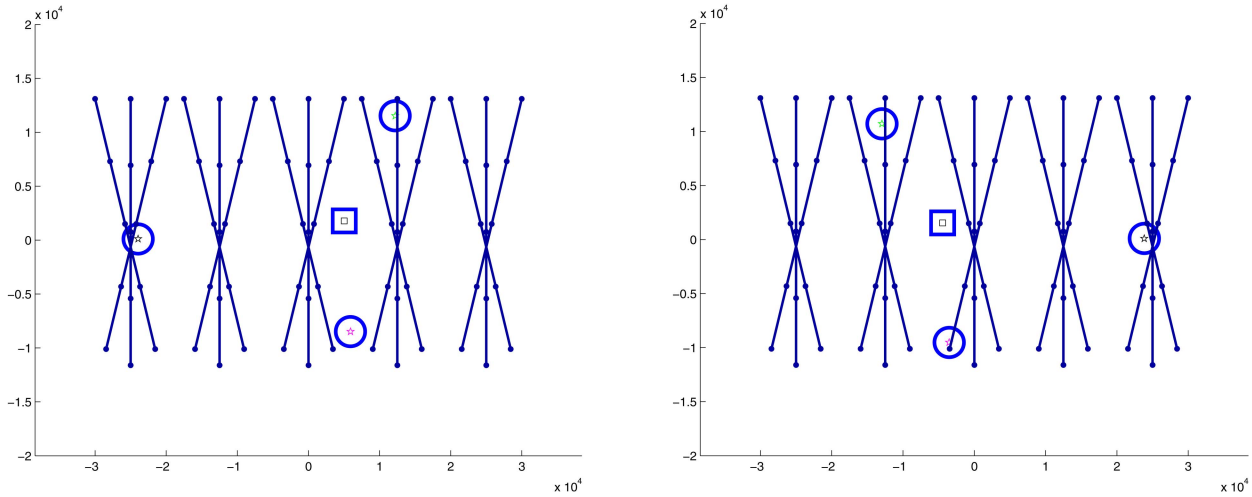

Fig. 10. Equivalent solutions: convergence results for two different runs. Interestingly, the geometries are "mirrors" of each other.

TABLE II
LFM Waveform is used
Scores of Trajectories for Figs. 9–10
(worst scores of each case are shown in bold)

Trajectory No.	1S-3R Fig. 9	1S-3R Fig. 10-left	1S-3R Fig. 10-right
1	52.14	48.51	47.90
2	**52.29**	41.66	52.18
3	47.15	**51.81**	51.08
4	38.91	42.41	30.10
5	36.93	41.49	33.29
6	35.97	43.20	33.82
7	46.56	29.69	34.65
8	51.09	31.91	30.73
9	47.04	29.47	35.12
10	35.60	32.07	42.70
11	35.63	30.51	40.14
12	41.67	29.59	40.53
13	45.51	49.65	**52.21**
14	50.49	50.43	42.29
15	51.86	45.64	47.81

waveform is available. Nonetheless, we use scores in our comparison tables, since they are easier to compare than the values of determinants of the information matrices.

A. Two-Node Cases

We look at the same two systems as before. The optimal placements are given in Figs. 11 and 12. This time the sensors are in the west-east orientation. This is again intuitive since the penetrating target provides high range rate (Doppler) measurement, and hence the information provided to tracker is higher. The complementarity of the waveforms is consistent with the complementarity of the optimal solutions. Another important observation is that the scores from the faster target are much better (lower) than the other one. This indicates that the Doppler information is so dominant that even though the slow target has many more waypoints and hence many more chances to be detected, it is harder to detect it if only a CW waveform is used.

B. Multiple Node Cases

Convergence geometry for the 1 source—3 receivers configuration is given in Fig. 13 in the fast-target case. It is similar to the regular triangle geometry. The eminent structure of the optimal geometry is to put two of the receivers close to both sides of the barrier, and the remaining receiver is placed in the center so that it forms a line with the source in north-south orientation. (The results are similar in the slow-target case.)

More important, this placement does not contradict the one from LFM case. It seems that both high Doppler detection and high target strength detection is possible if 3 source/receiver pairs are available.

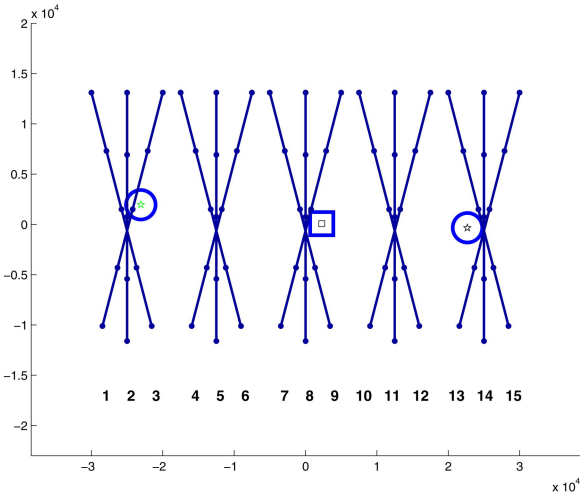

Fig. 11. CW waveform is used: Orientation of the sensors are complementary to the one of LFM waveform. See Table III for the scores. Target speed is high: 10 knots.

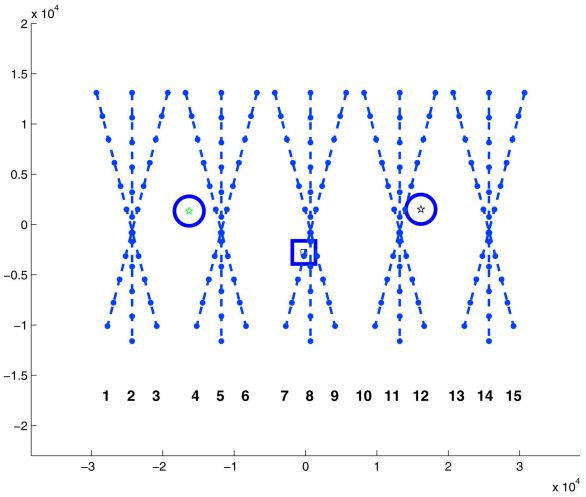

Fig. 12. CW waveform is used: Target speed is 4 knots.

Note that scores for slow target trajectories are worse than faster ones. Indeed, target SNR is considerably higher when target speed is high, resulting in much higher probability of detection, and also better localization. This effect is so dominant that even the fact that slow targets have twice as many waypoints is little help to the tracker.

6. PLACEMENT STRATEGIES WITH BOTH CW AND LFM WAVEFORMS

In the previous two sections, we have analyzed the proposed methodology and reported that the results are consistent with intuition. In this section, we assume the multistatic system is capable of using both waveforms and the target speed is unknown. Hence we consider two extreme cases to analyze the worst-case scenario: a target with 4 knots speed which is hard to detect with a CW waveform and a fast target moving with 10 knots trying to pass the barrier as quickly as possible. Each

TABLE III
Scores of Trajectories of Figures
(worst cases are shown bold)
Scores when CW Waveform is used for the Systems in the Figs. 11 and 12

Trajectory No.	Fast 10 kts	Slow 4 kts
1	4.73	91.63
2	11.72	95.17
3	9.23	84.09
4	7.12	33.39
5	6.27	44.36
6	7.62	23.98
7	11.09	96.03
8	10.19	84.77
9	**11.73**	**96.56**
10	8.07	23.57
11	6.18	44.98
12	8.51	33.77
13	8.18	85.76
14	10.97	96.52
15	8.62	93.18

Note: The slow target gives higher (worse) scores, unlike when an LFM waveform is used.

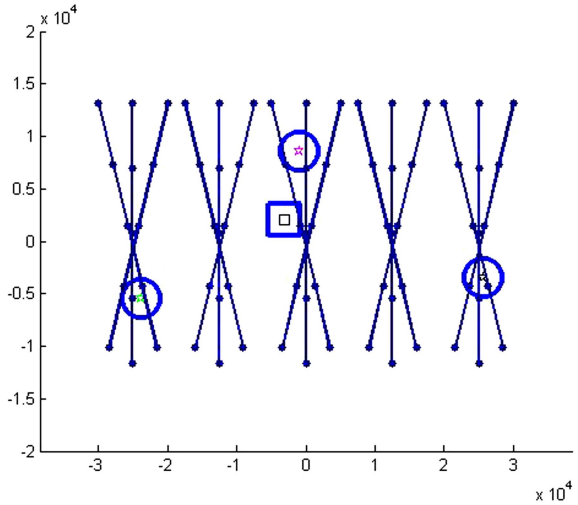

Fig. 13. CW waveform is used: Two of the receivers reach to the sides of the barrier and the source is in the middle with the third receiver.

of the 15 trajectories are duplicated so one trajectory corresponds to a slow target and the other corresponds to a fast one.

For the single source, three receivers case the optimal placement is shown in Fig. 14. The outcome is consistent with the earlier findings so that two of the receivers are placed far out and the third receiver stays in the middle of the barrier close to the source.

7. SENSITIVITY ANALYSIS OF SENSOR PLACEMENT RESULTS

In the previous sections, we have reported "optimal" placement strategies based on a sparsely sampled linear

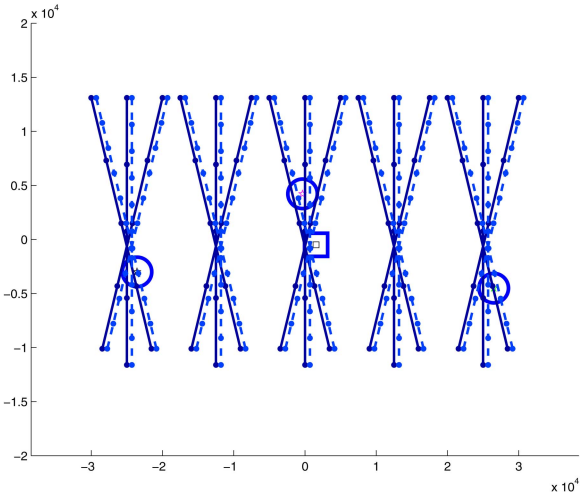

Fig. 14. Both CW and LFM waveforms are available. Trajectories are duplicated corresponding to different target speeds, 4 kts and 10 kts. The geometry is consistent with the earlier placements.

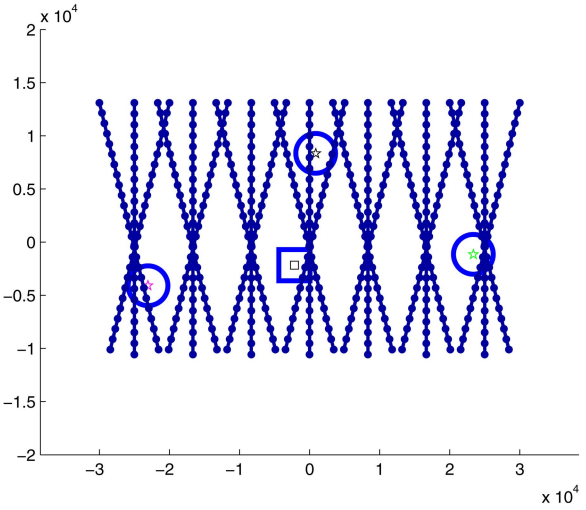

Fig. 15. The same initial placement as for Fig. 9, but with many more trajectories. The optimal placement is the same.

target trajectories. Here we investigate whether this choice has a dramatic impact on our results. The first analysis we consider is to use the result from Fig. 9 and run the optimization again with more trajectories, each of which has many more waypoints. The initial placement is the one in the optimization run resulting in Fig. 9. As seen in Fig. 15, the outcome is almost identical to the former result.

For the second analysis the trajectories are perturbed a random amount as seen in Fig. 16, and the optimization algorithms re-run. The initial placement for optimization is chosen as the optimal placement from Fig. 9. If this placement is optimal, it is expected that perturbation of the target trajectories would have little impact. The result in Fig. 16 confirms this.

In an overt network, there is no reason for a threat target to follow a straight line. Hence, in the last part of sensitivity analysis we consider piece-wise linear tra-

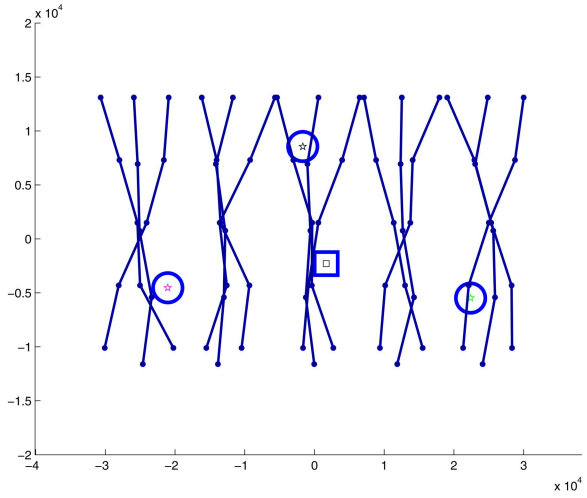

Fig. 16. The optimal placement with perturbed trajectories. The initial point is the optimal placement from Fig. 9.

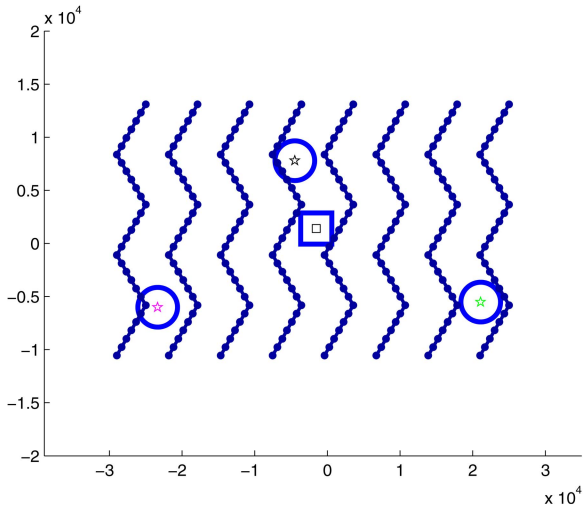

Fig. 17. Targets follow a zig-zag path. It appears that the optimal placement is robust.

jectories: such a trajectory is of interest since the target strength is changing along the trajectory. The result is given in Fig. 17. It appears that the optimal placement from Fig. 9 is robust for different configurations of target trajectories.

8. SUMMARY AND CONCLUSIONS

We propose an optimization technique for the optimal sensor placement for multistatic sonar systems. We study optimal placements in the LFM-only case, the CW-only case, and the combined LFM-CW case, and show that the optimal placements are consistent with our intuition, thus validating our placement methodology and its use as a placement aid in more complex scenarios where intuition is challenged.

An important aspect of the algorithm is that we employ a "minimax" criterion which results in a balanced surveillance performance. This makes sure that there is no path across the barrier for a target yet it remains "unseen."

Some aspects of modeling are important:

- Targets are not "point" targets: we employ an aspect angle dependent target strength model.
- Target Doppler is included in the localization analysis whenever CW waveforms are used.
- It is assumed that targets follow some realistic trajectories; Hence, availability of two complementary waveforms, CW and LFM, is incorporated in the metric.
- The modeling reflects the "Blanking Zone" due to direct blast signal reception.
- Signal Excess is calculated by a model where:
  —A simplified reverberation-limited sonar equation is used;
  —The Q-function is considered, which quantifies the Doppler performance of sonar waveforms in rejecting reverberation.

A scalar metric blends all of the above into a trajectory score, where "information gain" is computed at each waypoint of the trajectory. A steepest ascent algorithm is used for optimization, together with an intelligent step-size selection scheme (Armijo rule), and numerical gradient evaluation techniques.

It is desired to show that the "optimal" placements do, in fact, improve tracking performance. Thus, in future work, we plan to compare actual tracking performance based on optimal sensor placements with performance based on sub-optimal placements. This study would provide further validation that our information-based optimization objective captures the salient dataset characteristics that are required for high-quality tracker outputs and an effective surveillance system.

REFERENCES

[1] D. Bertsekas
Nonlinear Programming.
Athena Scientific, 1999.

[2] W. Burdic
Underwater Acoustic System Analysis.
Prentice Hall, 1984.

[3] S. Coraluppi
Multistatic sonar localization.
IEEE Journal on Oceanic Engineering, **31**, 4 (Oct. 2006).

[4] S. Coraluppi, C. Carthel, D. Hughes, A. Baldacci and M. Micheli
Multi-waveform active sonar tracking.
Proceedings of International Waveform Diversity and Design Conference, Pisa, Italy, June 2007.

[5] H. Cox
Fundamentals of Bistatic Active Sonar in Underwater Acoustic Data Processing.
Kluwer Academic Publishers, 1989.

[6] O. Erdinc, J. Areta, S. Coraluppi and P. Willett
Multistatic sonar sensor placement—A tracking perspective.
Proceedings of 2005 SPIE Conference on Signal and Data Processing of Small Targets, San Diego CA, Aug. 2005.

[7] O. Erdinc, P. Willett and S. Coraluppi
Multistatic sensor placement: A tracking approach.
Proceedings of International Conference on Information Fusion, Florence, Italy, July 2006.

[8] D. Grimmett
Multi-sensor placement to exploit complementary properties of diverse sonar waveforms.
Proceedings of International Conference on Information Fusion, Florence, Italy, July 2006.

[9] D. Grimmett and S. Coraluppi
Sensitivity analysis for multistatic LFAS localization accuracy.
NURC Technical Report SR-386, 2004.

[10] M. L. Hernandez and P. R. Horridge
Advances in the management of multi-sensor systmes with associated applications.
IEE, Target Tracking 2004: Algorithms and Allocations, May 23–24, 2004.

[11] P. R. Horridge and M. L. Hernandez
Multistatic radar resource management.
Proceedings of SPIE Signal and Data Processing of Small Targets, San Diego, CA, Aug. 2003.

[12] R. Niu, P. Willett and Y. Bar-Shalom
Matrix CRLB scaling due to measurements of uncertain origin.
IEEE Transactions on Signal Processing, **49**, 7 (2001), 1325–1335.

[13] C. Rago, P. Willett and Y. Bar-Shalom
Detection-tracking performance with combined waveforms.
IEEE Transactions on Aerospace and Electronic Systems, **34**, 2 (Apr. 1998), 612–624.

[14] M. van Velzen and L. Leutelt
Evaluation of radial receive array performance.
NURC Technical Report SR-400, Oct. 2004.

Ozgur Erdinc received the B.Sc. degree from Istanbul Technical University, Turkey, in 1997, and M.Sc. degree from University of Connecticut, Storrs, CT in 2004.

He is currently a research assistant/Ph.D. student in the Electrical and Computer Engineering department at the University of Connecticut. His primary research interests are in the areas of target tracking, signal processing, detection and estimation.

Peter Willett received his BASc (Engineering Science) from the University of Toronto in 1982, and his PhD degree from Princeton University in 1986. He has been a faculty member at the University of Connecticut ever since, and since 1998 has been a Professor. He was awarded IEEE Fellow status effective 2003. His primary areas of research have been statistical signal processing, detection, machine learning, data fusion and tracking. He also has interests in and has published in the areas of change/abnormality detection, optical pattern recognition, communications and industrial/security condition monitoring. He is editor-in-chief for IEEE Transactions on Aerospace and Electronic Systems, and until recently was associate editor for three active journals—IEEE Transactions on Aerospace and Electronic Systems (for Data Fusion and Target Tracking) and IEEE Transactions on Systems, Man, and Cybernetics, parts A and B. He is also associate editor for the IEEE AES Magazine, associate editor for ISIF's electronic Journal of Advances in Information Fusion, is a member of the editorial board of IEEE's Signal Processing Magazine and was first editor of the AES Magazine's periodic Tutorial issues. He has been a member of the IEEE AESS Board of Governors since 2003. He was General Co-Chair (with Stefano Coraluppi) for the 2006 ISIF/IEEE Fusion Conference in Florence, Italy and for the 2008 ISIF/IEEE Fusion Conference in Cologne, Germany, Program Co-Chair (with Eugene Santos) for the 2003 IEEE SMCC inWashington DC, and Program Co-Chair (with Pramod Varshney) for the 1999 Fusion Conference in Sunnyvale.

Stefano Coraluppi received the B.S. degree in Electrical Engineering and Mathematics from Carnegie Mellon University (Pittsburgh PA) in 1990, and the M.S. and Ph.D. degrees in Electrical Engineering from the University of Maryland (College Park MD) in 1992 and 1997, specializing in automatic control. From 1997 to 2002 he was a Senior Research Engineer at ALPHATECH Inc. (Burlington MA), where he worked on multi-sensor data fusion and target tracking for ground surveillance. In 2002 he joined the NATO Undersea Research Centre (La Spezia, Italy) as a Senior Scientist, and works on multistatic active sonar fusion and tracking for maritime surveillance. He served as General Co-chair of the *9th International Conference on Information Fusion* in Florence, Italy, in July 2006. He is an Associate Editor for Target Tracking and Multisensor Systems for the *IEEE Transactions on Aerospace and Electronic Systems*, and is a member of the Board of Directors of the *International Society of Information Fusion*.